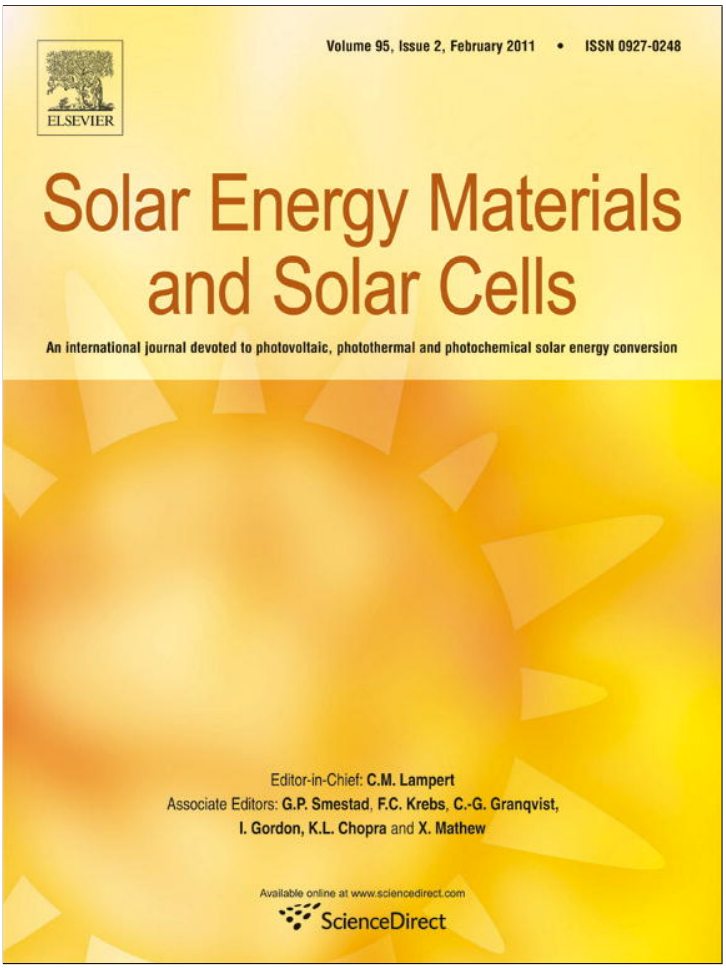

Solar Energy Materials & Solar Cells 95 (2011) 669–676

Contents lists available at ScienceDirect

Solar Energy Materials & Solar Cells

journal homepage: www.elsevier.com/locate/solmat

Antireflective characteristics of disordered GaAs subwavelength structures by thermally dewetted Au nanoparticles

J.W. Leem [a], J.S. Yu [a,*], Y.M. Song [b], Y.T. Lee [b]

[a] Department of Electronics and Radio Engineering, Kyung Hee University, Yongin 446-701, Republic of Korea
[b] Department of Information and Communications, Gwangju Institute of Science and Technology, Gwangju 500-712, Republic of Korea

ARTICLE INFO

Article history:
Received 4 June 2010
Accepted 30 September 2010
Available online 3 November 2010

Keywords:
Disordered subwavelength structures
Antireflective characteristics
Thermal dewetting
Au nanoparticles
GaAs

ABSTRACT

We report the antireflective characteristics of disordered subwavelength structures (SWSs) fabricated on a GaAs substrate by thermal dewetting induced Au nanoparticle masks in a subsequent inductively coupled plasma etching process. The optical reflectance relies on the geometric profile of disordered GaAs SWSs. The average size of Au nanoparticles and the correlation distance between adjacent nanoparticles are determined by the Au film thickness and the thermal dewetting condition. It is found that the height and shape of the SWSs, which can be controlled by changing the etching parameters, affect the reflectance strongly. The tapered SWS with a height of ~380 nm results in a relatively low reflectance spectra of $< \sim 5\%$ in the wavelength range of 350–900 nm. The angle-dependent reflectance is also investigated for the fabricated GaAs SWSs.

1. Introduction

Antireflection coatings (ARCs) have been widely used to realize high efficiency in optical components and optoelectronic devices by eliminating unwanted surface reflections. Recently, subwavelength gratings (SWGs), which are inspired by the moth-eye effect [1], have attracted increasing interest for various antireflection applications instead of single- or multilayer thin films [2–4]. The SWG structures, which have a period sufficiently smaller than the wavelength of light, can be used as ARCs [5]. The structure suppresses all higher orders of diffraction, satisfying the zeroth-order diffraction condition. Unfortunately, the fabrication of periodic subwavelength antireflective structures, such as SWGs, requires expensive and complicated processes, including e-beam lithography and nanoimprint lithography for nano-scale etch mask patterns [6,7]. Also, periodic nanostructures formed using silica or polystyrene monolayer colloidal crystals were reported for use in antireflection gratings [8,9]. However, these techniques have the disadvantages of low throughput and small patternable area.

On the other hand, metallic nanoparticles, which can be formed by a thermal dewetting process of metal thin films without the nanolithographic techniques, are of great interest for nanopatterns because they allow simple and low-cost fabrication over a large area [10,11]. The metallic nanoparticles, as etch masks, enable tailoring of disordered subwavelength structures (SWSs), thus providing antireflective properties [12]. Antireflective characteristics of the SWS depend strongly on its dimensions and geometric shape [13]. For high-efficiency solar cell applications, broadband wide-angle ARCs are required. The subwavelength antireflective structures were demonstrated to improve the performance in Si and organic solar cells though surface recombination can be enhanced [14–16]. For SWSs, the surface recombination effect would be relatively low compared to the nanowires and nanorods. Gallium arsenide (GaAs) is a key semiconductor material in device applications, such as solar cells, vertical cavity surface emitting lasers, and photodetectors. Although several studies were made on the SWSs of silicon, gallium nitride, silicon nitride, etc. [15,17,18], there has been very little work reported on that of GaAs. The addition of subwavelength surface structures is expected to increase the light trapping and absorption in GaAs-based solar cells [19,20]. In this paper, the antireflective characteristics of disordered GaAs SWSs, by thermally dewetted Au nanoparticles under different dewetting conditions and subsequent inductively coupled plasma (ICP) etching using $SiCl_4$ gas at various etching conditions, were systematically investigated. The angle dependence of reflectance was also studied in the GaAs SWSs.

2. Experimental details

A schematic diagram of process steps for fabricating the GaAs SWSs by thermal dewetting of Au thin films and ICP etching is shown in Fig. 1. The Au thin films of 5, 10, and 15 nm were evaporated on a (1 0 0) GaAs substrate with size 25×25 mm^2 by thermal evaporation. Prior to evaporation, the native oxides at the

* Corresponding author.
E-mail address: jsyu@khu.ac.kr (J.S. Yu).

0927-0248/$ - see front matter © 2010 Elsevier B.V. All rights reserved.
doi:10.1016/j.solmat.2010.09.038

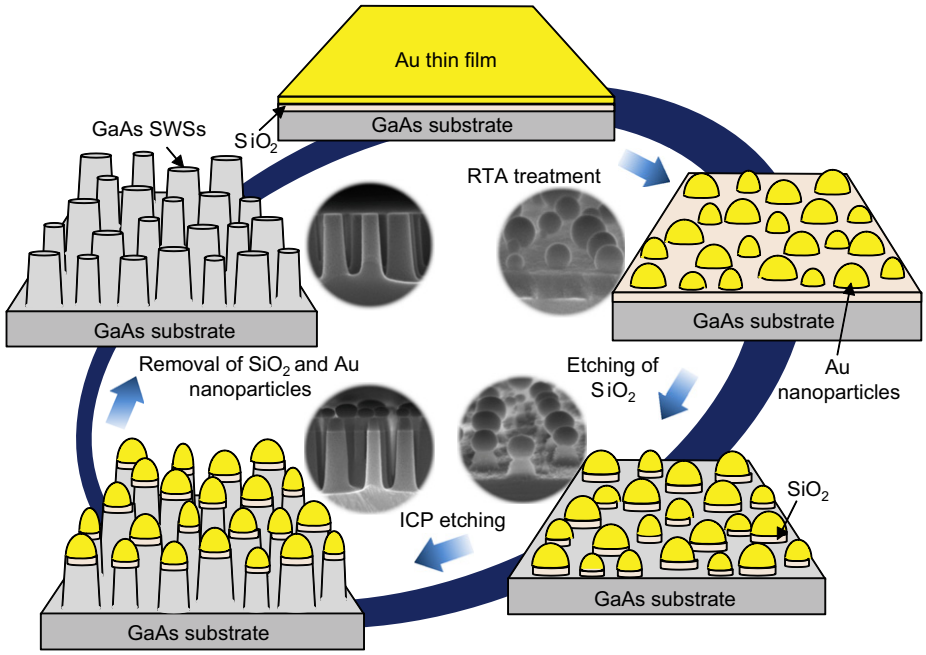

Fig. 1. Schematic diagram of process steps for fabricating the GaAs SWSs by thermal dewetting of Au thin films and ICP etching.

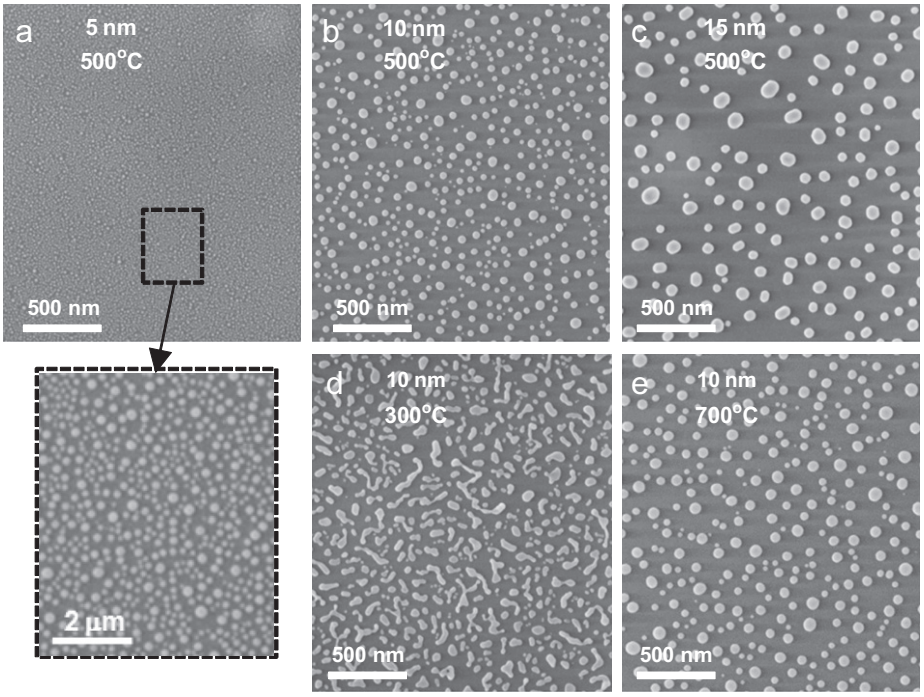

Fig. 2. Top-view SEM images of the dewetted Au nanopatterns after RTA at 500 °C for the Au films of (a) 5 nm, (b) 10 nm, and (c) 15 nm, and after RTA at (d) 300 °C and (e) 700 °C for the Au film of 10 nm. For more distinction between Au nanoparticles, the SEM image of (a) was magnified.

substrate surface were removed. A 50 nm-thick SiO_2 buffer layer was deposited by plasma enhanced chemical vapor deposition. The evaporation rate and thickness were monitored by a quartz crystal oscillator technique. To form the desired Au nanopatterns, the samples were treated thermally by rapid thermal annealing (RTA) at various temperatures of 300, 500, and 700 °C in a nitrogen environment. The RTA time was fixed at 100 s. During the RTA process, the Au thin films were agglomerated into the nanosized particles through the dewetting process. The SiO_2 layer was etched in CF_4 plasma by reactive ion etch system using the thermally dewetted Au nanopatterns as an etch mask. Using the Au/SiO_2 nanomasks, the GaAs SWSs were fabricated by an inductively coupled plasma (ICP) etch system using $SiCl_4$ gas with or without additional Ar gas. The etching parameters, such as RF power, ICP power, process pressure, flow rate of additional Ar gas, and etching time, were varied to achieve a desirable etching profile of GaAs SWSs for broadband antireflective characteristics. After dry etching, the remaining Au and SiO_2 residues were removed by an Au etchant and a buffered oxide etchant, respectively. The etched profile, etched depth, and surface

morphology of the fabricated GaAs SWSs were characterized by a field-emission scanning electron microscope (FE-SEM). The reflectance property was evaluated using a UV-VIS-NIR spectrophotometer (Cary 500, Varian) with an integrating sphere for the total (specularly and diffusely) reflected light collection, i.e., hemispherical reflectance measurement. To prevent the specular component from escaping out of the entrance port on the integrating sphere, the samples were mounted onto its backside with an angle of $\sim 8^{\circ}$ with respect to the incident light. The angle-dependent reflectance was measured using a Cary variable angle specular reflectance accessory in the specular mode.

3. Results and discussion

Fig. 2 shows the top-view SEM images of the dewetted Au nanopatterns after RTA at 500 °C for the Au films of (a) 5 nm, (b) 10 nm, and (c) 15 nm, and after RTA at (d) 300 °C and (e) 700 °C for the Au film of 10 nm. For more distinction between Au nanoparticles, the SEM image of (a) was magnified. Thermal dewetting and agglomeration occur to minimize the surface free energy when the surface energy of Au metal films is larger than the interfacial energy and the surface energy of the underlying substrate in the high temperature heating process [21]. On using the 50 nm-thick SiO_2 buffer layer, the Au–SiO_2 interface properties favor the development of suitably structured metal islands more than an Au–GaAs interface. This can be explained by the fact that the Au film is unstable on the SiO_2 layer with a relatively low surface energy [10]. It is somewhat difficult to form the desirable metal islands on GaAs substrate without the SiO_2 buffer layer because the surface energy of Au metal films is much lower than that of the GaAs substrate. The nanopattern geometry is strongly affected by the thickness of Au films at a given RTA temperature. The size of nanoparticles becomes larger and the correlation distance between adjacent nanoparticles increases as the Au film thickness is increased. The average diameter and correlation distance were estimated using a commercial image processor (ImageJ 1.42q, NIH). The average diameters of Au nanoparticles were increased from 24.1 ± 16.3 nm at 5 nm of Au films to 136.6 ± 101.9 nm at 15 nm after RTA at 500 °C. The average correlation distances were 63.8, 101.2, and 226.5 nm for 5, 10, and 15 nm Au films, respectively. For thicker Au films, the islands get bigger and the correlation distance becomes larger because the Au nanoclusters merge together, thus reducing the density. As shown

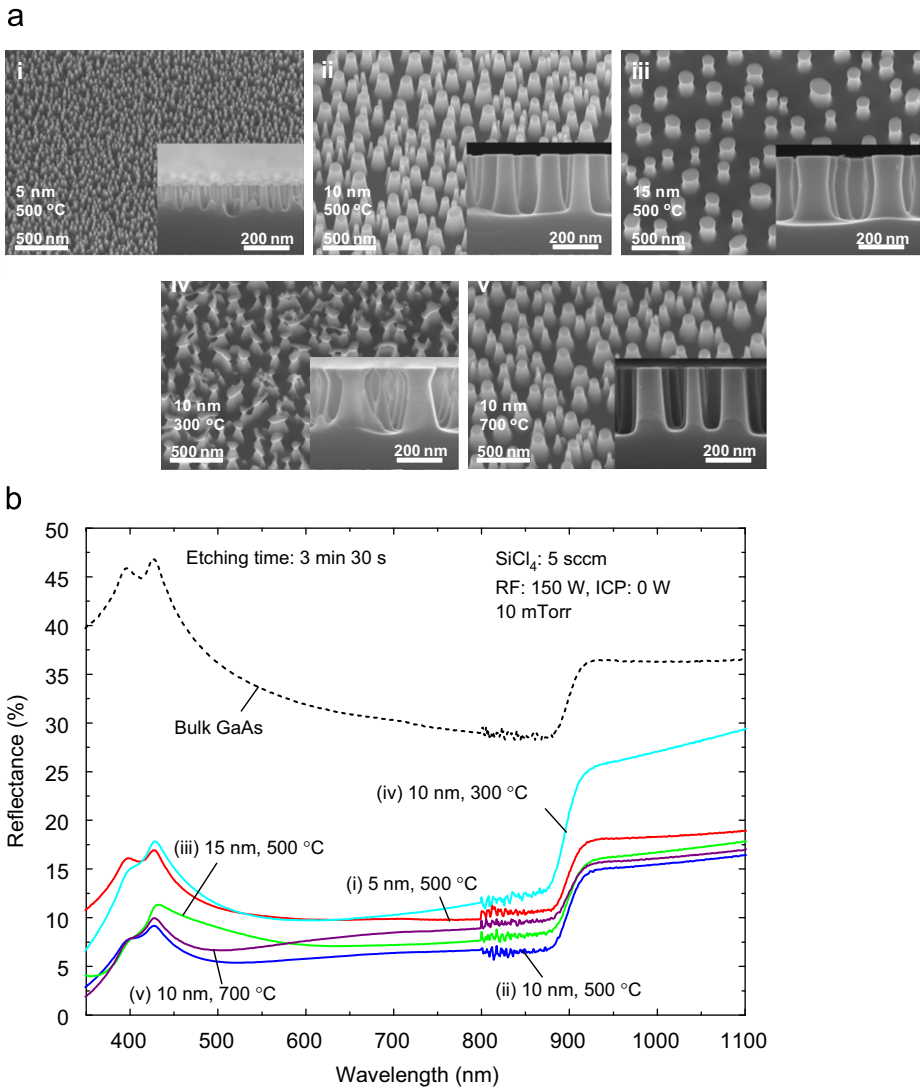

Fig. 3. (a) SEM images and (b) reflectance spectra of the GaAs SWSs etched with the Au nanomask patterns after RTA at 500 °C for the Au films of (i) 5 nm, (ii) 10 nm, and (iii) 15 nm, and after RTA at (iv) 300 °C and (v) 700 °C for the Au film of 10 nm. Insets of (a) show the cross-sectional SEM images of the fabricated GaAs SWSs. For comparison, the reflectance of bulk GaAs substrate is also shown in (b).

in Fig. 2(d), the 10 nm Au film was not completely dewetted after RTA at 300 °C because the thermal energy was not sufficient. At a temperature of 700 °C, the average size of nanoparticles and the correlation distance were slightly increased to 89.8 ± 78.5 and 119.4 nm, respectively, compared to those at 500 °C in Fig. 2(b). This means that agglomeration is enhanced with increasing temperature. Clearly, the Au nanoparticles are not properly formed for nanomask patterns if the Au film is too thick or the temperature is too low.

Fig. 3 shows (a) SEM images and (b) reflectance spectra of GaAs SWSs etched with the Au nanomask patterns after RTA at 500 °C for the Au films of (i) 5 nm, (ii) 10 nm, and (iii) 15 nm, and after RTA at (iv) 300 °C and (v) 700 °C for the Au film of 10 nm. The insets show cross-sectional SEM images of the fabricated GaAs SWSs. The etching of GaAs substrate was performed with 150 W RF power and 0 W ICP power at 10 mTorr for 3 min 30 s in 5 sccm $SiCl_4$ plasma. As can be seen in Fig. 3(a), the Au nanomask patterns were transferred directly onto the GaAs substrate by ICP etching. The etched depths of GaAs SWSs were obtained as 102.4 ± 18.3, 286.6 ± 7.5, and 302.2 ± 5.8 nm for Au films of 5, 10, and 15 nm, respectively. The etched profile became tapered as the pattern density was increased. The etch rate is reduced in higher density patterns with smaller diameters due to the low influx of ions and radicals. For the dewetted nanopatterns of the 10 nm Au film at 300 °C, the etched profiles have sidewall undercuts. The reflectance spectrum is strongly dependent on the etched profiles of GaAs SWSs.

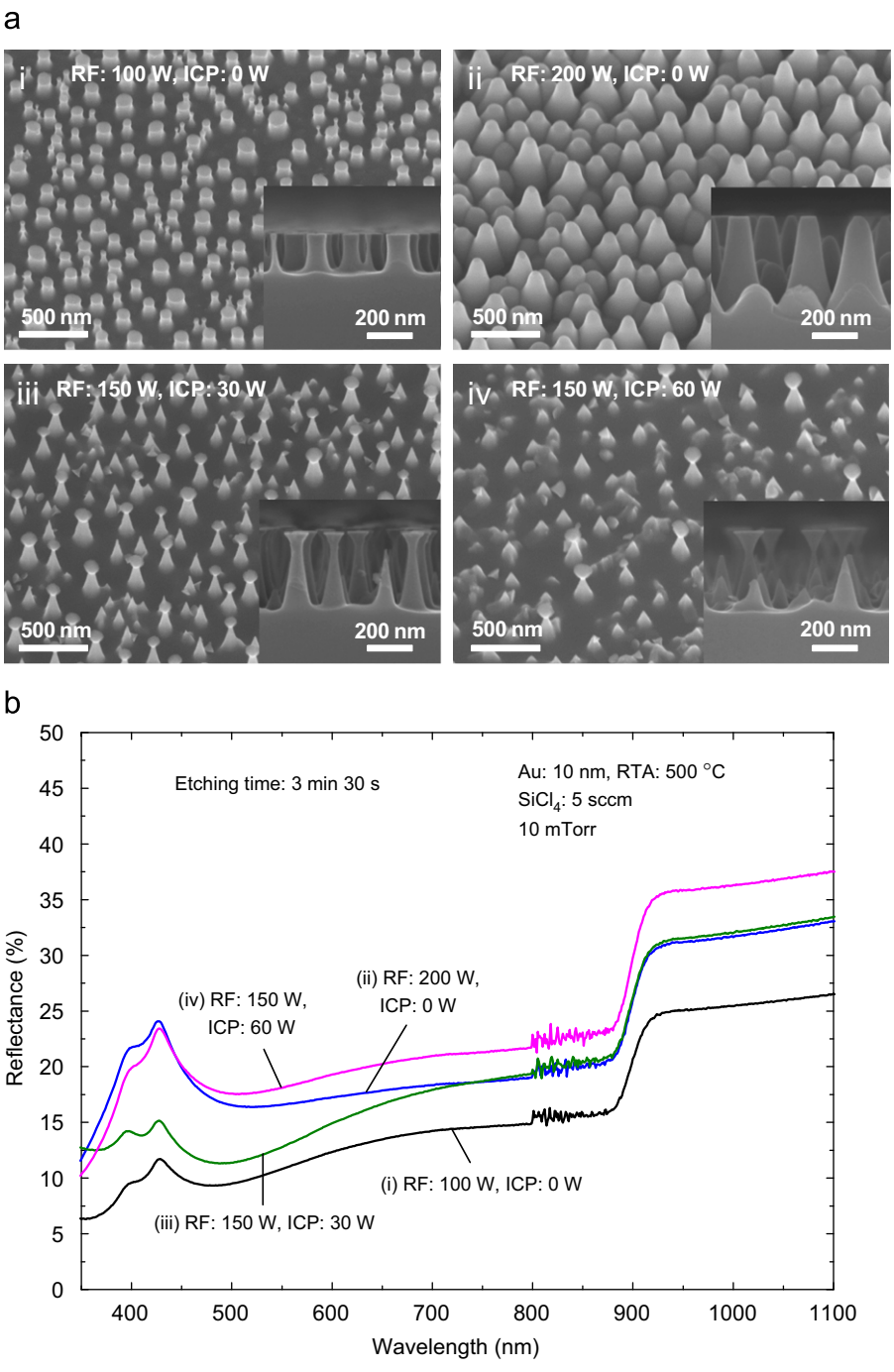

Fig. 4. SEM images of the fabricated GaAs SWSs with RF powers of (a) 100 W and (b) 200 W, and with additional ICP powers of (c) 30 W and (d) 60 W to the RF power of 150 W using the dewetted nanomask patterns of the 10 nm Au film at 500 °C. Inset shows the cross-sectional SEM images of the fabricated GaAs SWSs.

For comparison, the reflectance of bulk GaAs substrate is also shown in Fig. 3(b), exhibiting values higher than ~30% at wavelengths of 350–1100 nm. The reflectance was significantly reduced for GaAs SWSs compared to that of the bulk GaAs. Above $\lambda \sim 880$ nm, there exist abrupt increases in reflectance for all samples including the GaAs substrate. This can be explained by backscattering of light by the reflection from the back surface of the GaAs substrate because of its optical transparency below the energy bandgap of GaAs [22]. For the GaAs SWS with sidewall undercuts, the reflectance was increased, especially in the long wavelength range. The SWS with small size and low height produced increased reflectance despite the high density. The dewetted nanopatterns after RTA at 500 °C for the 10 nm Au film were optimized, indicating the lowest reflectance of the fabricated GaAs SWS.

Fig. 4(a) shows SEM images of the fabricated GaAs SWSs with RF powers of (i) 100 W and (ii) 200 W, and additional ICP powers of (iii) 30 W and (iv) 60 W to the RF power of 150 W using the dewetted nanopatterns of the 10 nm Au film at 500 °C. The samples were etched with 5 sccm $SiCl_4$ at 10 mTorr for 3 min 30 s.

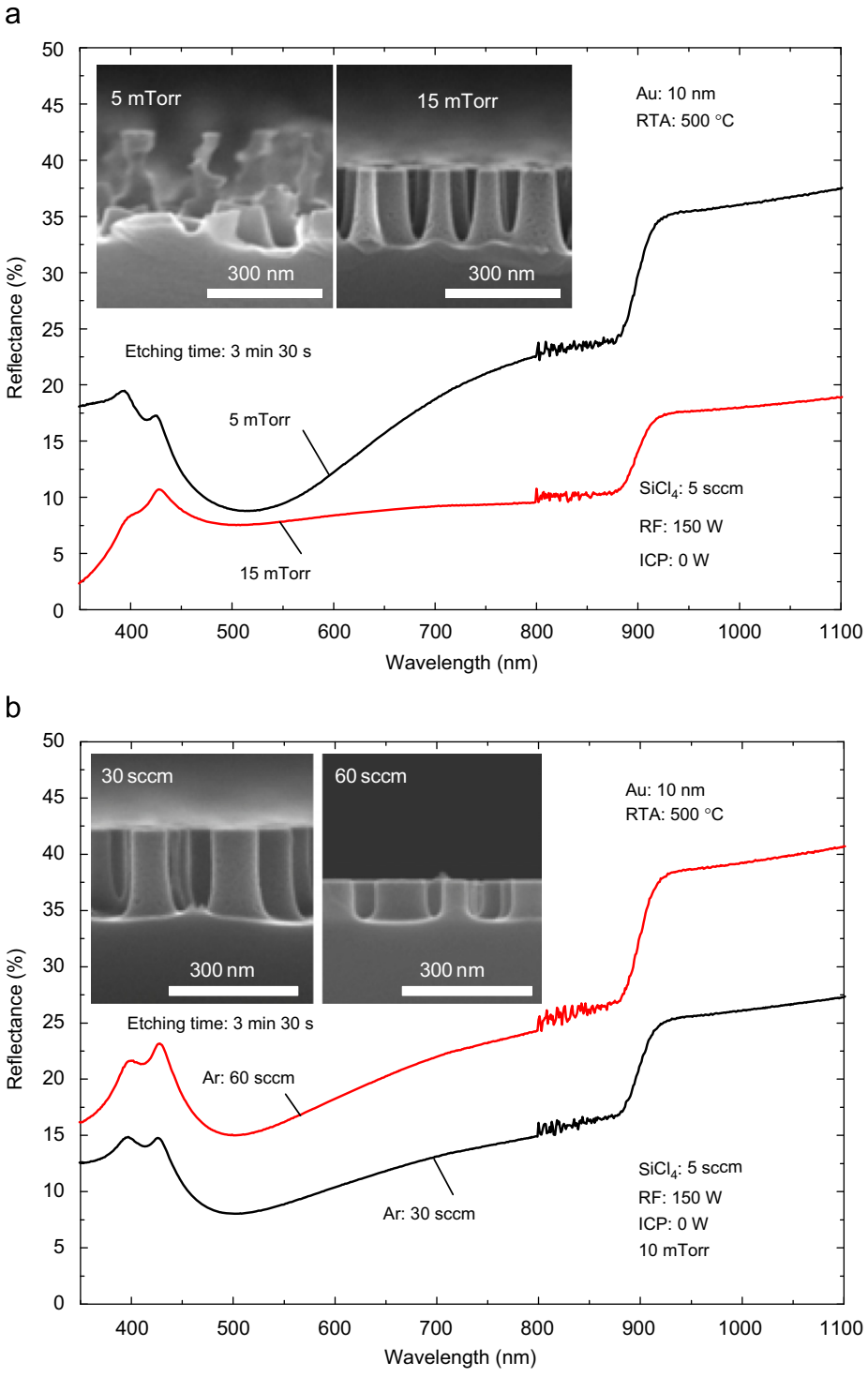

Fig. 5. Reflectance spectra of the GaAs SWSs etched at (a) different process pressures and (b) different Ar flow rates using the dewetted nanomask patterns of the 10 nm Au film at 500 °C. Insets show the SEM images of the fabricated GaAs SWSs.

The etched shape of GaAs SWS was dependent on the RF and ICP powers. The etch depth was decreased and the structure became less tapered at the RF power of 100 W. The height of SWSs was increased as the RF power was increased. At a high RF power of 200 W, the etched depth was increased but etching occurred even in the masked regions. The etched features with rounded tops were increased because the Au nanomask was gradually removed from edges during the etching process under high RF power. The addition of ICP power created the undercut sidewall beneath the mask due to enhanced lateral etching as shown in (iii) of Fig. 4(a). A further increase in ICP power (i.e., 60 W ICP power, in addition to 150 W RF power (iv)) leads to an apparent disconnection of undercut parts and the structure partly collapsed. The corresponding reflectance as a function of wavelength is shown in Fig. 4(b). The SWS structure with lower height, etched at 100 W RF power, exhibited higher reflectance values, especially in the long wavelength range, compared to the etched structure in Fig. 3(b). The increase in rounded features raised the reflectance. In our previous work [23], theoretical analysis was carried out using the rigorous coupled-wave analysis method for periodic GaAs SWGs with truncated cone profiles. From the simulation results, the reflectance is reduced with increasing height, which is roughly consistent with that of the disordered SWSs in this experiment. To suppress effectively the surface reflection, the tapered profile of SWSs is desirable because it provides a more graded effective index between the GaAs and air [24]. With the increase in ICP power, the reflectance increased due to the lower density and the higher height by the enhanced undercut and collapse. The additional ICP power rather degraded the reflectance performance of GaAs SWSs.

The effect of (a) process pressure and (b) Ar flow rate on the reflectance spectrum of the GaAs SWSs etched using the dewetted nanomask patterns of the 10 nm Au film at 500 °C is shown in Fig. 5. SEM images of the fabricated GaAs SWSs are shown in the insets. At high process pressure, the etch rate decreases. The etch depth was reduced at 15 mTorr, indicating a higher reflectance spectrum. At a low process pressure of 5 mTorr, the etched profile of the SWS was deformed because the etch masking fails by excessive lateral etching. The reflectance spectrum was largely changed and it increased significantly in the short and long wavelength regions. As shown in the SEM images of Fig. 5(b), the additional Ar gas results in a vertical etch profile. However, the etch depth became lower for a higher Ar flow rate (i.e., 60 sccm). This indicates that the etch rate decreases as Ar gas is added to $SiCl_4$ gas. The vertical-shape like pillars have higher reflectance values than the tapered shape. Moreover, the lower height caused a further increase in reflectance. Thus, the significant increase in reflectance is attributed to the vertical sidewalls with a relatively low height.

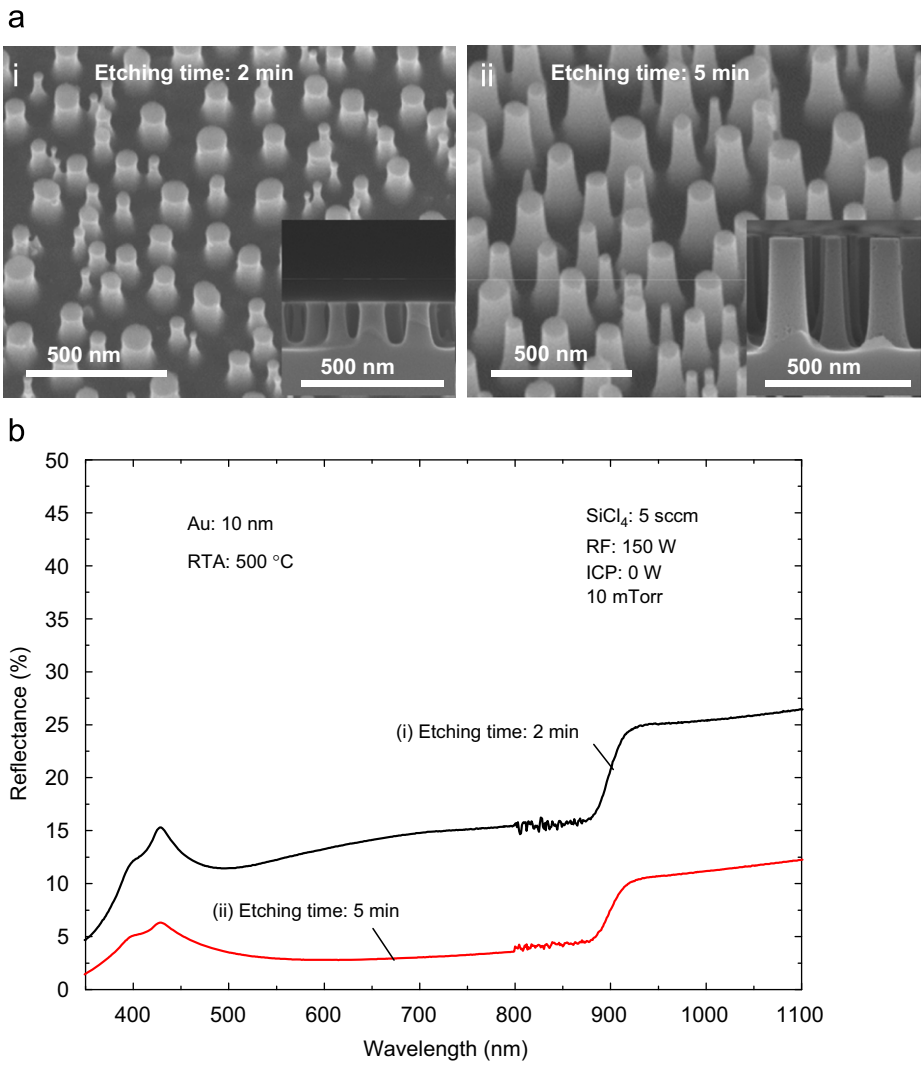

Fig. 6. (a) SEM images and (b) reflectance spectra of the GaAs SWSs etched using the dewetted nanomask patterns of the 10 nm Au film at 500 °C for (i) 2 min and (ii) 5 min.

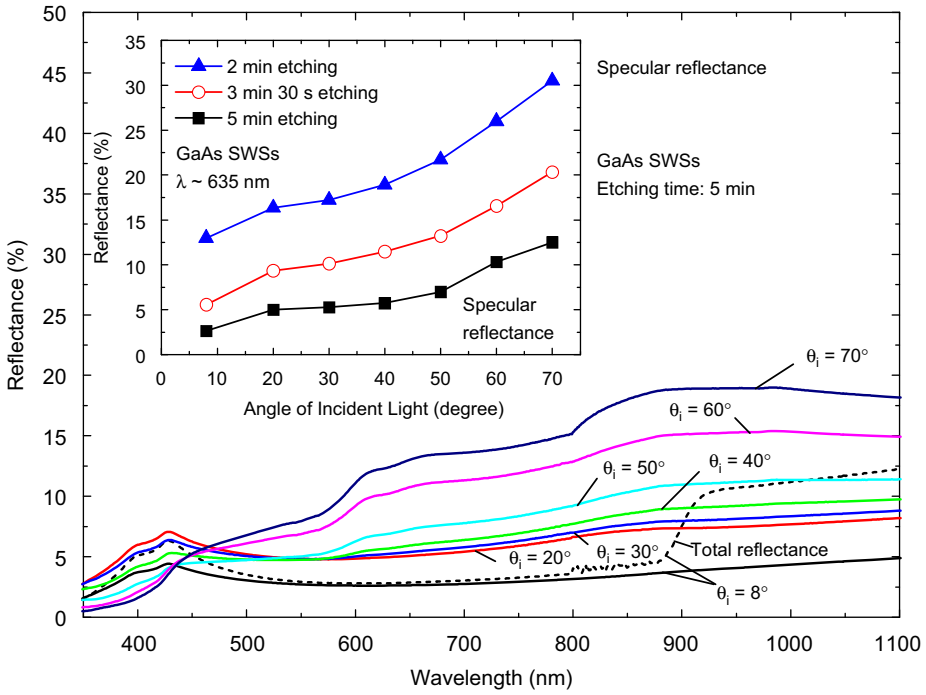

Fig. 7. Specular reflectance spectra at different incident light angles of θ_i=8–70° for the GaAs SWS etched for 5 min. For comparison, the total reflectance spectrum is shown by the dashed line at θ_i=8°. Inset shows angle-dependent specular reflectance of the GaAs SWSs etched for different etching times at a wavelength of 635 nm.

Fig. 6 shows (a) SEM images and (b) reflectance spectra of GaAs SWSs etched using the dewetted nanomask patterns of the 10 nm Au film at 500 °C for (i) 2 min and (ii) 5 min. It is evident that etch rate increases as the etching time increases. The etched depth almost linearly increased from 151 nm for 2 min to 383 nm for 5 min, i.e., an etch rate of ~77.3 nm/min. On increasing the etching time, the etch depth of GaAs SWSs increased and the structure was more tapered because the lateral etching under the Au nanomask was slightly enhanced. When the etching time became shorter, from 3 min 30 s to 2 min, reflectance increased. After an etch for 5 min, the reflectance significantly reduced to $<\sim$5% in the wavelength region of 350–900 nm. Therefore it is expected that the GaAs SWS with higher height will further improve the antireflective properties over a wide wavelength range.

Fig. 7 shows the specular reflectance spectra at different incident light angles of θ_i=8–70° for the GaAs SWS etched for 5 min. For comparison, the total reflectance spectrum is shown by the dashed line at θ_i=8°. In the specular mode, measurement was taken at a low angle of incidence (i.e., ~8°), close to normal incidence so that the incident beam is not blocked by the detector. It is noticeable that the specular and total reflectance values are almost the same in the wavelength range between 500 and 880 nm. There is a deviation between specular and hemispherical reflectance measurement results at $\lambda<500$ nm due to diffuse scattering. The scattering may increase and also be relevant at a longer wavelength if the incident angle is increased. At wavelengths longer than 880 nm, the discrepancy is attributed to the backscattered light from the back surface as mentioned above. The reflectance increased with increasing incident angle and it rapidly rose especially at $\theta_i>50°$. The reflectance was less than 9.2% at wavelengths $<$800 nm up to θ_i=50° for the 5 min-etched sample. The angle-dependent specular reflectance of the GaAs SWSs etched for different etching times at a wavelength of 635 nm is shown in the inset of Fig. 7. The angle-dependent reflectance is strongly dependent on the height of SWSs. The reflectance increased from 13% to 30.5% for the 2 min-etched sample as the incident angle increased from 8° to 70°. For the 5 min-etched sample, the reflectance increased from 2.6% at θ_i=8° to 12.5% at θ_i=70°. Consequently, the disordered GaAs SWSs with taller and tapered shape led to a relatively low reflectance spectrum over a wide angle of incident light.

4. Conclusion

We fabricated the disordered GaAs SWSs on a GaAs substrate using self-assembled Au nanoparticles by thermal dewetting as etch masks and subsequent ICP etching in $SiCl_4$ plasma with/without Ar addition to suppress their surface reflection. After RTA of the 10 nm Au film at 500 °C for 100 s, the density and size of Au nanopatterns were optimized to achieve the lowest reflectance of the SWS. By using the optimized Au nanomasks, the ICP etching was performed by changing various etching conditions, such as RF/ICP power, process pressure, and etching time, for efficient antireflective characteristics. It is found that the reflectance depends strongly on height and sidewall shape of the SWS. The relatively tall and tapered SWS exhibited a lower reflectance spectrum. The surface reflectance of GaAs was largely decreased, indicating a low value of $<$5% at wavelengths of 350–900 nm, by optimizing the SWG structure. For the SWS with a height of ~380 nm, a reflectance less than 9.2% at wavelengths $<$800 nm for θ_i=8–50° was obtained. This approach, which uses thermally dewetted nanoparticle masks for the fabrication of SWSs, is cost-effective and scalable to large areas, unlike e-beam lithography. These results can provide a promising potential of GaAs SWSs as ARCs for efficient solar cells.

Acknowledgements

The work was supported by the Korea Science and Engineering Foundation (KOSEF) Grant funded by the Ministry of Education, Science and Technology (MEST) (No. 2010-0016930).

Reference

[1] P.B. Clapham, M.C. Hutley, Reduction of lens reflexion by the "Moth Eye" principle, Nature 244 (1973) 281–282.

[2] P. Lalanne, G.M. Morris, Antireflection behavior of silicon subwavelength periodic structures for visible light, Nanotechnology 8 (1997) 53–56.

[3] Y.M. Song, J.S. Yu, Y.T. Lee, Antireflective submicrometer gratings on thin-film silicon solar cells for light-absorption enhancement, Opt. Lett. 35 (2010) 276–278.

[4] Y.M. Song, S.J. Jang, J.S. Yu, Y.T. Lee, Bioinspired parabola subwavelength structures for improved broadband antireflection, Small 6 (2010) 984–987.

[5] A. Gombert, W. Glaubitt, K. Rose, J. Dreibholz, B. Bläsi, A. Heinzel, D. Sporn, W. Döll, V. Wittwer, Subwavelength-structured antireflective surfaces on glass, Thin Solid Films 351 (1999) 73–78.

[6] K. Wensun, S.C. Huang, A. Kechiantz, C.P. Lee, Subwavelength gratings fabricated on semiconductor substrates via E-beam lithography and lift-off method, Opt. Quantum Electron. 37 (2005) 425–432.

[7] Y. Kanamori, K. Hane, Broadband antireflection subwavelength gratings for polymethyl methacrylate fabricated with molding technique, Opt. Rev. 9 (2002) 183–185.

[8] C.H. Sun, B.J. Ho, B. Jiang, P. Jiang, Biomimetic subwavelength antireflective gratings on GaAs, Opt. Lett. 33 (2008) 2224–2226.

[9] Y. Li, J. Zhang, B. Yang, Antireflective surfaces based on biomimetic nanopillared arrays, Nano Today 5 (2010) 117–127.

[10] J.M. Lee, B.I. Kim, Thermal dewetting of Pt thin film: etch-masks for the fabrication of semiconductor nanostructures, Mater. Sci. Eng. A 449–451 (2007) 769–773.

[11] Y.M. Song, E.S. Choi, J.S. Yu, Y.T. Lee, Light-extraction enhancement of red AlGaInP light-emitting diodes with antireflective subwavelength structures, Opt. Express 17 (2009) 20991–20997.

[12] K. Nishioka, S. Horita, K. Ohdaira, H. Matsumura, Antireflection subwavelength structure of silicon surface formed by wet process using catalysis of single nano-sized gold particle, Sol. Energy Mater. Sol. Cells 92 (2008) 919–922.

[13] S.A. Boden, D.M. Bagnall, Tunable reflection minima of nanostructured antireflective surfaces, Appl. Phys. Lett. 93 (2008) 133108-3.

[14] H. Sai, H. Fujii, K. Arafune, Y. Ohshita, Y. Kanamori, H. Yugami, M. Yamaguchi, Wide-angle antireflection effect of subwavelength structures for solar cells, Jpn. J. Appl. Phys. 46 (2007) 3333–3336.

[15] K.C. Sahoo, M.K. Lin, E.Y. Chang, Y.Y. Lu, C.C. Chen, J.H. Huang, C.W. Chang, Fabrication of antireflective sub-wavelength structures on silicon nitride using nano cluster mask for solar cell application, Nanoscale Res. Lett. 4 (2009) 680–683.

[16] K. Forberich, G. Dennler, M.C. Scharber, K. Hingerl, T. Fromherz, C.J. Brabec, Performance improvement of organic solar cells with moth eye anti-reflection coating, Thin Solid Films 516 (2008) 7167–7170.

[17] S. Wang, X.Z. Yu, H.T. Fan, Simple lithographic approach for subwavelength structure antireflection, Appl. Phys. Lett. 91 (2007) 061105-3.

[18] C.H. Chiu, P. Yu, H.C. Kuo, C.C. Chen, T.C. Lu, S.C. Wang, S.H. Hsu, Y.J. Cheng, Y.C. Chang, Broadband and omnidirectional antireflection employing disordered GaN nanopillars, Opt. Express 16 (2008) 8748–8754.

[19] P. Yu, C.H. Chang, C.H. Chiu, C.S. Yang, J.C. Yu, H.C. Kuo, S.H. Hsu, Y.C. Chang, Efficiency enhancement of GaAs photovoltaics employing antireflective indium tin oxide nanocolumns, Adv. Mater. 21 (2009) 1618–1621.

[20] M.A. Tsa, P. Yu, C.H. Chiu, H.C. Kuo, T.C. Lu, High efficiency InGaP/GaAs solar cell with sub-wavelength structure on AlInP window layer, in: Proceedings of the Third IEEE International Nanoelectronics Conference, Hong Kong, 2010, pp. 781–782.

[21] D.J. Srolovitz, M.G. Goldiner, The thermodynamics and kinetics of film agglomeration, J. Miner. Met. Mater. Soc. 47 (1995) 31–36.

[22] M.L. Kuo, D.J. Poxson, Y.S. Kim, F.W. Mont, J.K. Kim, E.F. Schubert, S.Y. Lin, Realization of a near-perfect antireflection coating for silicon solar energy utilization, Opt. Lett. 33 (2008) 2527–2529.

[23] Y.M. Song, S.Y. Bae, J.S. Yu, Y.T. Lee, Closely packed and aspect-ratio-controlled antireflection subwavelength gratings on GaAs using a lenslike shape transfer, Opt. Lett. 34 (2009) 1702–1704.

[24] S. Chattopadhyay, Y.F. Huang, Y.J. Jen, A. Ganguly, K.H. Chen, L.C. Chen, Anti-reflecting and photonic nanostructures, Mater. Sci. Eng. R 69 (2010) 1–35.